

Patrick Minnis, Erika Geier, Bruce A. Wielicki
Atmospheric Sciences, NASA Langley Research Center, Hampton, VA 23681

Sunny Sun-Mack, Yan Chen, Qing Z. Trepte
SAIC, Hampton, VA 23666

Xiquan Dong
University of North Dakota, Grand Forks, ND

David R. Doelling, J. Kirk Ayers, Mandana M. Khaiyer
AS&M, Hampton, VA 23666

1. INTRODUCTION

Simultaneous measurement of radiation and cloud fields on a global basis is recognized as a key component in understanding and modeling the interaction between clouds and radiation at the top of the atmosphere, at the surface, and within the atmosphere. The NASA Clouds and Earth's Radiant Energy System (CERES) Project (Wielicki et al., 1998) began addressing this issue in 1998 with its first broadband shortwave and longwave scanner on the Tropical Rainfall Measuring Mission (TRMM). This was followed by the launch of two CERES scanners each on *Terra* and *Aqua* during late 1999 and early 2002, respectively. When combined, these satellites should provide the most comprehensive global characterization of clouds and radiation to date. Unfortunately, the TRMM scanner failed during late 1998. The *Terra* and *Aqua* scanners continue to operate, however, providing measurements at a minimum of 4 local times each day.

CERES was designed to scan in tandem with high-resolution imagers so that the cloud conditions could be evaluated for every CERES measurement. The cloud properties are essential for converting CERES radiances shortwave albedo and longwave fluxes needed to define the radiation budget (ERB). They are also needed to unravel the impact of clouds on the ERB. The 5-channel, 2-km Visible Infrared Scanner (VIRS) on the TRMM and the 36-channel 1-km Moderate Resolution Imaging Spectroradiometer (MODIS) on *Terra* and *Aqua* are analyzed to define the cloud properties for each CERES footprint. To minimize inter-satellite differences and aid the development of useful climate-scale measurements, it was necessary to ensure that each satellite imager is calibrated in a fashion consistent with its counterpart on the other CERES satellites (Minnis et al., 2006) and that the algorithms are as similar as possible for all of the imagers. Thus, a set of cloud detection and retrieval algorithms were developed that could be applied to all three imagers utilizing as few channels as possible while producing stable and accurate cloud properties.

*Corresponding author address: Patrick Minnis, NASA Langley Research Center, MS 420, Hampton, VA 23681-2199. email: p.minnis@nasa.gov.

This paper discusses the algorithms and results of applying those techniques to more than 5 years of *Terra* MODIS, 3 years of *Aqua* MODIS, and 4 years of TRMM VIRS data.

2. DATA

Although the TRMM VIRS continues to operate, only data from January 1998 - July 2001 have been analyzed so far. The VIRS 0.65, 1.64, 3.75, 11.0, and 12.0 μm bands are used in the cloud detection and retrievals. *Terra* MODIS began stable operations in late February 2000 and continues to operate satisfactorily. *Aqua* MODIS became operational in July 2002 and is also still scanning. To date, the CERES cloud analysis algorithms have been applied to *Terra* and *Aqua* Collection-4 MODIS data through August 2005. The 1-km MODIS data are sampled every other pixel and scan line to reduce processing time. The CERES-MODIS (CM) cloud analysis algorithms use the 0.65, 1.38, 1.64 (2.13), 3.8, 6.7, 8.5, 10.8, and 12.0 μm channels. The CERES scanners measure broadband shortwave, total, and infrared window (8-12 μm) radiances with a nadir footprint of ~ 20 km.

Auxiliary data consist of the CERES Meteorology, Ozone, and Aerosol (MOA) dataset which includes vertical profiles of temperature and humidity. The CERES MOA profiles are based on the European Center for Medium-range Weather Forecasting (ECMWF) reanalyses for VIRS and on the Global Modeling Assimilation Office GEOS 4.03 (DAO, 1997) for MODIS. Clear-sky albedos measured from VIRS and MODIS 0.65 and 1.6- μm data (Sun-Mack et al., 1999, 2003) are used with angular directional models to estimate the clear-sky reflectance for a given scene. The maps are updated each month. MODIS-based surface emissivities (Chen et al., 2002) are used in conjunction with the reanalysis skin temperatures to estimate the clear-sky infrared radiances. The MOA data are used for clear-sky radiance calculations. Topographic, surface type, snow and sea ice databases are also input for the analyses.

3. METHODOLOGIES

The cloud properties reported here are the results of applying the *Terra* Edition 2 (Ed2) and *Aqua* Edition 1 (Ed1) algorithms. These include cloud detection and retrievals. Each imager pixel is first classified as clear or

cloudy using updated versions of the CERES classification schemes that employ the 0.64 (visible), 1.6 or 2.1 (near infrared), 3.7 (solar infrared), 10.8 (infrared), and 12 (split window) μm radiances (Trepte et al., 1999, 2002). The 1.6- μm channel is used for the near-infrared data from VIRS and *Terra*, while the 2.1- μm channel is used for *Aqua* because of problems with the *Aqua* 1.6- μm channel. To detect cloudy pixels, the radiances are compared with the predicted clear-sky radiances in a series of cascading tests. The differences between the 1.6 and 2.1- μm reflectances for clear snow surfaces necessitated some adjustments to the cloud mask algorithms (Minnis et al., 2003). An improved polar cloud detection algorithm was instituted for *Aqua* Ed 1 resulting in some large discrepancies between *Terra* and *Aqua* in polar regions. The detection of thin cirrus was also improved in *Aqua* Ed1 with the use of the 1.38- μm channel reflectance (Trepte et al., 2006)

Effective droplet radius r_e or effective ice crystal diameter D_e , optical depth τ , ice or liquid water path IWP/LWP , cloud temperature T_c , height z_c , thickness, and cloud phase are derived from these same radiances using one of three different techniques. The visible infrared solar-infrared split-window technique (VISST), an updated version of the original 3-channel daytime method (Minnis et al., 1995), is used during daytime, which is defined as the time when the solar zenith angle SZA is less than 82° . At other times of day, the solar-infrared infrared split-window technique (SIST) is used to determine all of the parameters. The SIST, an improved version of the original 3-channel nighttime method (Minnis et al., 1995), only uses thermal and solar infrared data. Thus, its retrievals are valid only for optically thin clouds. When the SIST is used, default values are used for all parameters except phase, T_c , and z_c for clouds with $\tau < 8$. The third method, adapted from Platnick et al. (2001), is designated the solar-infrared infrared near-infrared technique (SINT) and is only applied to MODIS data during the daytime for clouds over snow or ice backgrounds. The 2.13- μm channel on *Aqua* is used instead of the 1.6- μm channel in the SINT. Determination of the background surface as snow or ice can either come from the scene classification for adjacent clear pixels or from the snow and ice maps used in the CERES data stream (Trepte et al., 2002). All of the methods compute both ice and liquid water solutions that simultaneously determine T_c , τ , and particle size. Each method iteratively matches the observed radiances to TOA radiances calculated using emittance and reflectance parameterizations that account for atmospheric attenuation and surface reflectance and emission. The cloud reflectances and emittances are included in the parameterizations (Minnis et al., 1998; Arduini et al., 2002) using updated lookup tables for each specific channel. The phase is selected based on the cloud temperatures, the availability of a solution, best consistency with a solution, and cloud altitude.

The pixel-level data are convolved with the individual broadband CERES radiative fluxes to obtain the Single Scanner Footprint (SSF) dataset. These SSF products include the cloud fraction and mean associated properties for up to two cloud layers. No cloud properties

could be retrieved for $\sim 6.7\%$ of pixels classified as cloudy during the daytime. At night, only 1.4% of the cloudy pixels yield no retrieval. Most no-retrieval pixels occur in polar regions over snow-covered surfaces or over very bright deserts. Over snow, the SINT is unable to find a match, probably because of uncertainties in the clear-sky reflectance fields. Over deserts, the pixels detected as clouds may actually be heavy concentrations of aerosols that are misclassified as clouds. Over most ocean and land areas outside the polar regions and Saharan Desert, the no-retrievals account for 1 - 2% of the total number of cloudy pixels. To account for the no-retrievals, the SSF convolution assigns the mean cloud properties from cloudy pixels in the footprint with retrieved values to the no-retrieval pixels, if more than 1/9 of pixels in the footprint have valid cloud retrievals. Otherwise, only the valid cloudy pixels are used and the no-retrieval pixels are not considered as part of the total number of pixels in the footprint.

4. RESULTS AND DISCUSSION

Imager pixel-level data are retained for data granules corresponding to a selected number of locations around the globe for visual assessment and for comparison to independent validation datasets obtained from several research facilities around the world. Figure 1 shows *Terra* CM 30x30 km² average values of r_e , τ , and LWP compared with 1-hr means derived from radar and radiometer data at the Atmospheric Radiation Measurement (ARM) Southern Great Plains site using the methods of Dong et al. (2002). Means for each variable are given in the top panels followed by the standard deviations. Linear correlation coefficients are given in the bottom panels. The two datasets correspond closely in most cases. The correlation coefficients for τ and LWP are quite high. Overall, the LWP and optical depth means differ by only 3 and 4%, respectively. The mean optical depth and LWP from *Aqua* (not shown) were 13% and 24% greater than the corresponding means from the SGP site for July 2002 - December 2004.

Effective radius values do not track as closely. On average, the ARM value of r_e is 0.6 μm larger than that from the CM retrieval. This surprising result is likely due to the fact that the *Terra* MODIS 3.8- μm channel measures brightness temperatures that are too large. Figure 2 shows a comparison of daytime 3.8- μm brightness temperatures from *Terra* and *Aqua* data taken over the Arctic during July 2005 and matched according to the methods of Minnis et al. (2002). The difference of 0.44 K is near the 5-year mean difference of 0.6 K, a value that corresponds to $\sim 0.6 \mu\text{m}$ in the retrieval of r_e . Thus, the *Terra* underestimate is probably due to the calibration. The mean values of r_e from *Aqua* and the SGP are both 8.2 μm (not shown).

A more limited comparison was performed using data from the ARM Mobile Facility microwave radiometer stationed at Pt. Reyes, CA during 2005. This site is located on the coast where marine stratus advects over the edge of continent. Thus, the measurements should be more representative of a marine environment. The

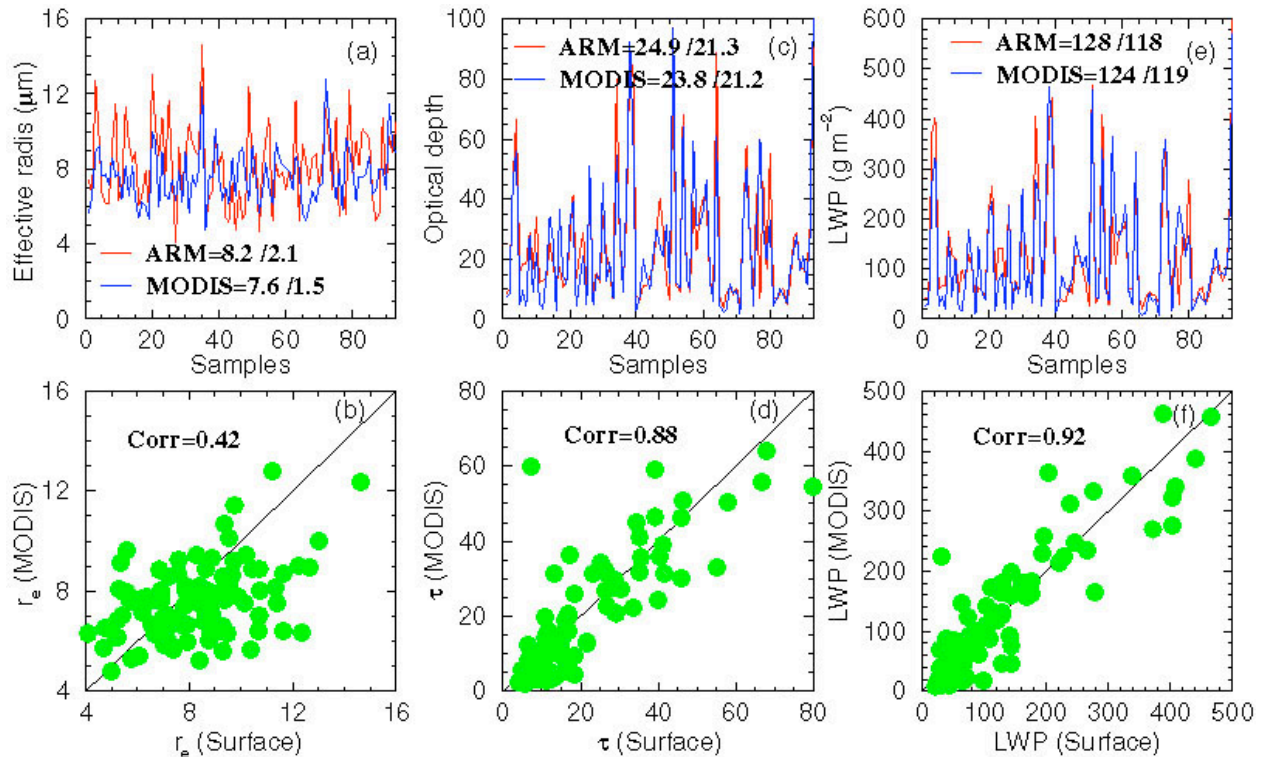


Fig. 1. Comparison of CERES Terra MODIS analyses and surface-based retrievals at ARM SGP Central Facility for single-layer stratus clouds, July 2002 - December 2004.

preliminary comparison is shown in Fig. 3 for 19 overcast single-layer stratus cases observed from *Terra* between February and June 2005. The results are similar to those over the SGP site with a mean difference of 8%. Similar comparisons have been performed for cirrus clouds at the SGP and elsewhere (Mace et al., 1995; Chiriaco et

al., 2006). In general, the CM method does not detect clouds with $\tau < 0.3$.

The low cloud heights over the SGP were also compared with radar and lidar retrievals at the Central facility. Figure 3 summarizes the comparisons. At night (top), the correlation coefficient is roughly double that found during the day (bottom panel). However, the mean differences between the cloud-top height from the surface and the effective height from the CM retrieval for *Terra* are nearly the same for both day and night, ~395 m. The effective height corresponds to a location near the physical center of the cloud. The standard deviation in the differences is approximately 1 km. The *Terra* effective temperatures average 0.24 K and 1.1 K less than the cloud-top temperatures determined from the radar and soundings at the SGP. Thus, the underestimate of cloud effective height is primarily a problem in converting cloud temperature to height. The CM methodology uses a lapse rate approach similar to that of Minnis et al. (1991) for assigning heights to boundary layer clouds. Over land, a 24-h running mean of surface temperature is used to anchor the lapse rate. If standard MOA temperature profiles were used, the boundary layer heights would be overestimated by 1 km or more because of problems in defining boundary layer inversions (e.g., Garreaud et al., 2001).

The stratus cloud effective heights from *Aqua* (not shown) were 580-m lower than the tops measured by the radar at the SGP during the daytime, but only 185-m lower at the night. During daytime, the *Aqua* effective

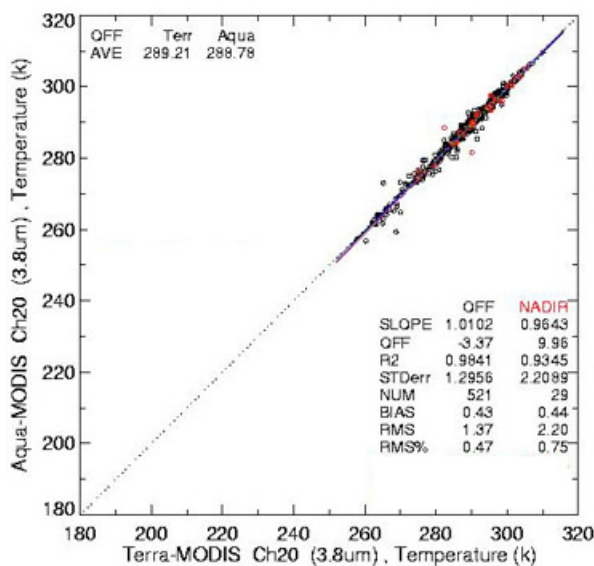


Fig. 1. Comparison of mean 3.8- μ m brightness temperatures from matched *Terra* and *Aqua* MODIS data from 0.5° regions over the Arctic during July 2005. Red points are at nadir, black points are from off-nadir.

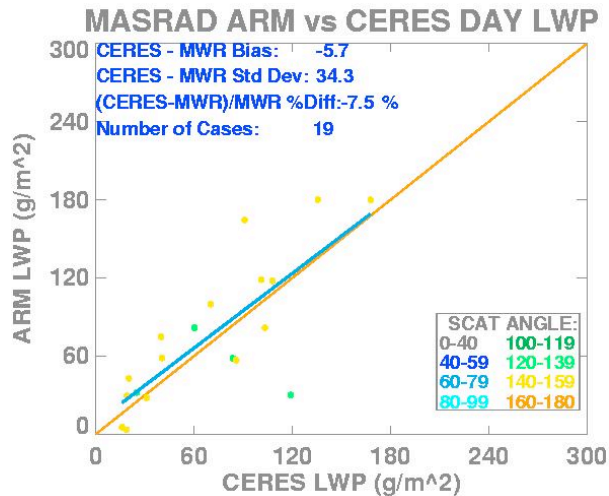


Fig. 3. Same as Fig. 1f, except over Pt. Reyes, CA, February - June 2005.

temperature is, on average, 0.6 K greater than that deduced from the surface data. The overestimate of effective temperature is mainly due to a few cases when the optical depth is relatively small and the temperature correction is not enough to account for the cloud's semi-transparency. At night, the CM *Aqua* temperatures are 2.4 K less than those from the surface. Cirrus cloud effective heights are typically between the cloud base and center as defined by the surface radar and lidar data (e.g., Mace et al., 2005).

Examples of the overall results can be found elsewhere (e.g., Minnis et al., 2002, 2003, 2004; Sun-Mack et al., 2006) along with comparisons to climatologies from surface and satellite observations. The MODIS Atmosphere Science Team (AST) is also generating cloud products from the same MODIS data as CERES, but using a different set of algorithms, models, and channels (King et al., 2003). It is important for users of either the CERES or AST MODIS cloud products to understand how the two results differ. Thus, some of examples of differences between the MODIS AST Collection-4 and CERES are presented here.

Figure 5 shows the mean daytime cloud fractions from *Aqua* for June 2004 from the CM analysis and the MYD08 Collection-4 average products from the MODIS AST. Overall, the patterns are very similar. However, the CERES values are larger over the Arctic Ocean and many land areas. The two methods yield nearly identical means over the northern midlatitude oceans, but over the remaining ocean areas and land areas like Venezuela, the Great Plains, India, southern Australia, and north central Africa, the MOD08 means are typically 0.05 - 0.20 greater than the cloud amounts from CERES.

Figure 6 shows the corresponding mean daytime cloud droplet radii. Again, the patterns are very similar, but some significant differences are evident. In general, MYD08 values are generally larger. Over the open ocean the differences are as great as 6 μm over large

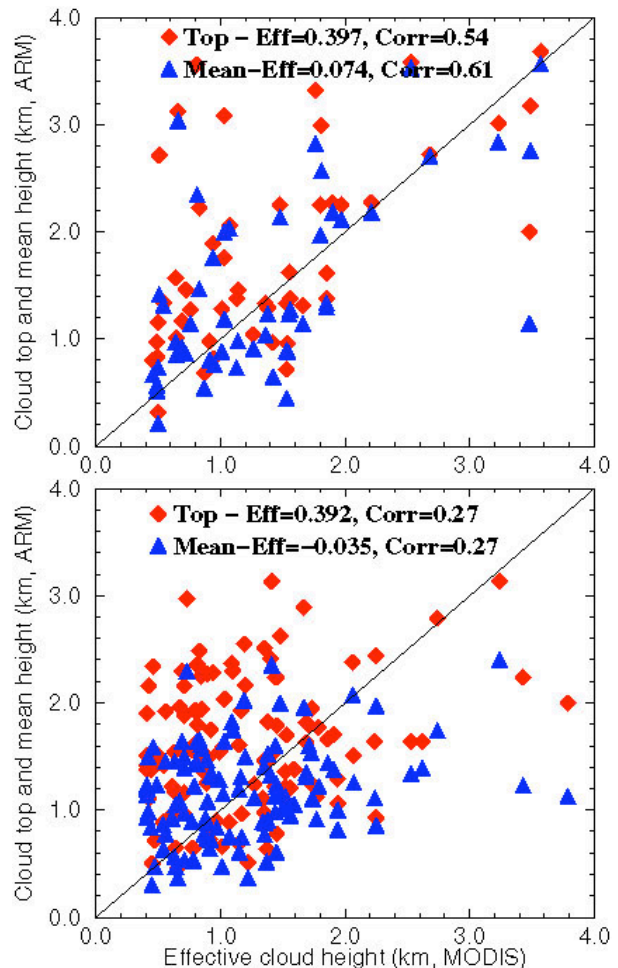


Fig. 4. Same as Fig. 1b, except for low cloud heights. Top: night. Bottom: day.

areas around the Intertropical Convergence Zones, the tropical warm pool (TWP), and in some trade cumulus regimes. The differences elsewhere over the ocean are on the order of 2 μm . Over land, the differences are typically 1 - 2 μm . The source of these differences is not known at this time, but may be due to the use of different solar constants and modeling differences.

Effective cloud temperatures from *Terra* are compared in Fig. 7 for October 2004. The colors are slightly different for the two images, however, the differences can be discerned. The patterns are mostly the same, but the MOD08 temperatures are slightly greater in the trade cumulus areas and over the deserts. Over the ITCZ and TWP, the CERES clouds tend to be colder, on average. The temperatures are similar poleward of 60°N.

The temperature differences translate to differences in effective cloud pressure as seen in Fig. 8. The CERES marine stratus clouds are at higher pressures than the MOD08 values, while the trade cumulus regions show the opposite behavior. The CERES mean cloud pressure over the TWP, ITCZ, and deserts is less than that from MOD08 by 50-100 hPa. Despite similar-

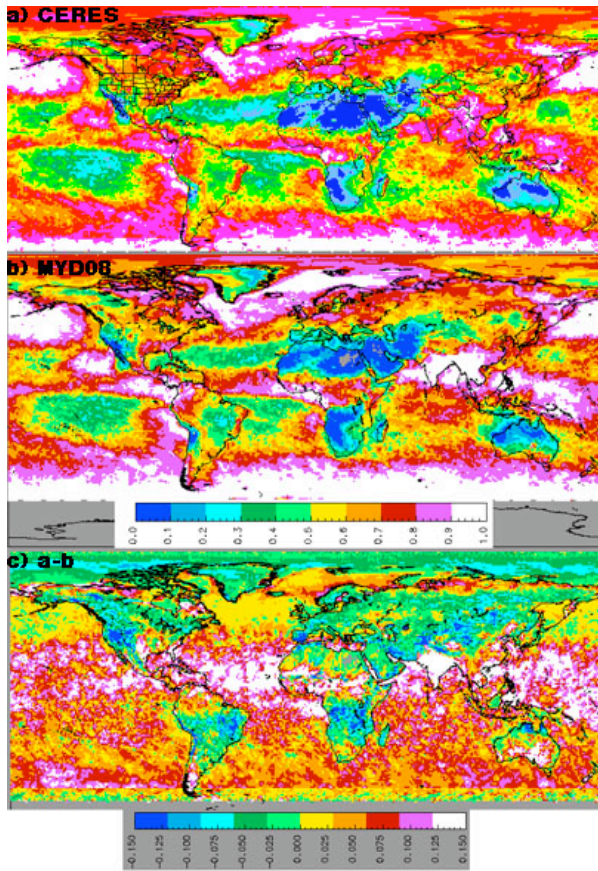


Fig. 5. Mean daytime cloud amounts from Aqua MODIS from (a) CM and (b) MODIS AST algorithms, June 2004. Differences in (c).

ities in cloud temperature over the Arctic, the CERES cloud pressures are greater than those from MOD08, probably as a result of applying the lapse rate method. Over India, Afghanistan, and Tibet, the CERES cloud pressures are dramatically less than the MOD08 results.

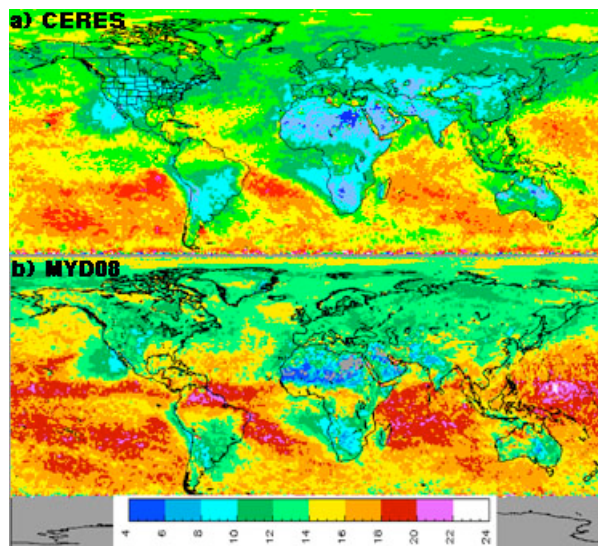


Fig. 6. Same as Fig. 5, except for effective water droplet radius (μm).

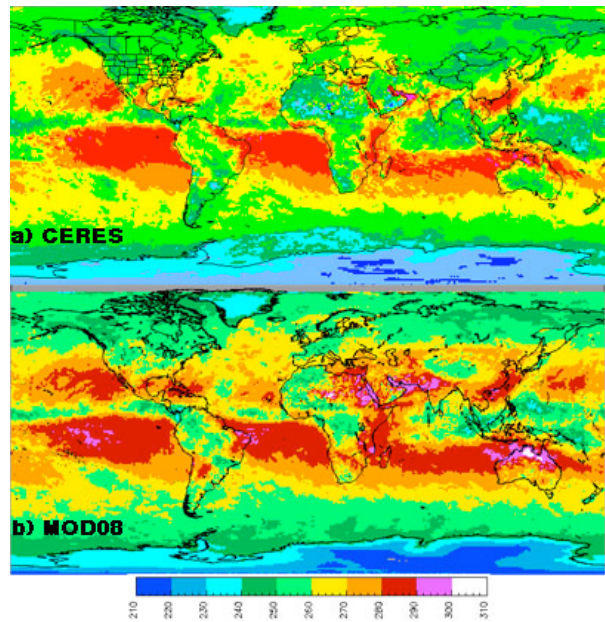


Fig. 7. Mean daytime effective cloud temperatures (K) from Terra MODIS from (a) CM and (b) AST, October 2004.

5. CONCLUDING REMARKS

The unique CERES cloud-radiation dataset now covers more than 5 years. Initial evaluations indicate that the cloud properties are of reasonable accuracy and will be useful for climate studies. Further validation and studies to understand the differences between the MODIS AST and CERES products are continuing. Because the MODIS data have been revised in the Collection-5 series, the CERES cloud products will be soon be reprocessed using Edition-3 algorithms, and analysis will continue for the life of the instruments.

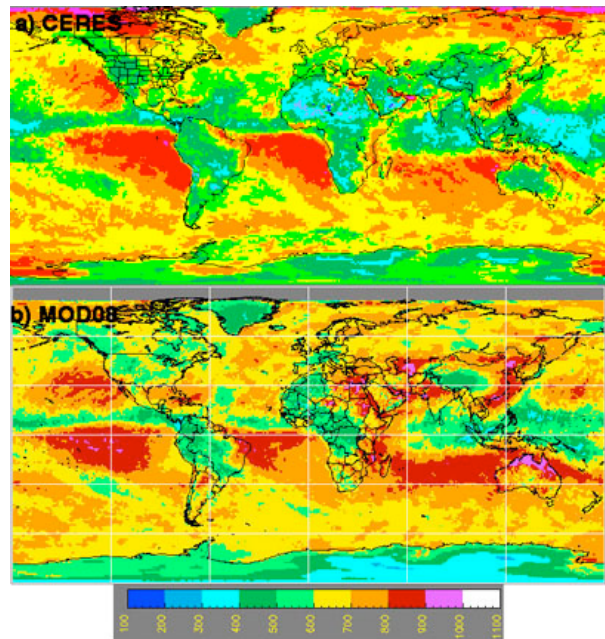


Fig. 8. Same as Fig. 7, but for effective cloud pressure (hPa).

ACKNOWLEDGEMENTS

This research was supported by the NASA Science Mission through the CERES Project. Thanks to Mark Miller for providing the ARM LWP data from Pt. Reyes, CA. The ARM SGP data were obtained from Department of Energy ARM archive.

REFERENCES

- Arduini, R. F., P. Minnis, and D. F. Young, 2002: Investigation of a visible reflectance parameterization for determining cloud properties in multi-layered clouds. *Proc. 11th AMS Conf. Cloud Physics.*, Ogden, UT, June 3-7, CD-ROM, P2.4.
- Chen, Y., S. Sun-Mack, P. Minnis, D. F. Young, and W. L. Smith, Jr., 2002: Surface spectral emissivity derived from MODIS data. *Proc. SPIE 3rd Intl. Asia-Pacific Environ. Remote Sensing Symp.: Remote Sens. of Atmos., Ocean, Environment, and Space*, Hangzhou, China, October 23-27, **4891**, 361-369.
- Chiriaco, M., H. Chepfer, P. Minnis, M. Haefelin, S. Platnick, D. Baumgardner, P. Dubuisson, M. McGill, V. Noel, J. Pelon, D. Spangenberg, S. Sun-Mack, and G. Wind, 2006: Comparison of CALIPSO-like, LaRC, and MODIS retrievals of ice cloud properties over SIRTa in France and Florida during CRYSTAL-FACE. In press, *J. Appl. Meteorol. Climatol.*
- DAO, 1997: GEOS-3 Data Assimilation System Architectural Design. *DAO Office Note 97-06*. Data Assimilation Office, Goddard Space Flight Center, Greenbelt, MD 20771.
- Dong, X., P. Minnis, G. G. Mace, W. L. Smith, Jr., M. Poellot, R. T. Marchand, and A. D. Rapp, 2002: Comparison of stratus cloud properties deduced from surface, GOES, and aircraft data during the March 2000 ARM Cloud IOP. *J. Atmos. Sci.*, **59**, 3256-3284.
- Garreaud, R. D., J. Rutllant, J. Quintana, J. Carrasco, and P. Minnis, 2001: CIMAR-5: A snapshot of the lower troposphere over the subtropical southeast Pacific. *Bull. Amer. Meteor. Soc.*, **92**, 2193-2208.
- King, M. D., W. P. Menzel, Y. J. Kaufman, D. Tanre, B. C. Gao, S. Platnick, S. A. Ackerman, L. A. Remer, R. Pincus, and P. A. Hubanks, 2003: Cloud and aerosol properties, precipitable water, and profiles of temperature and humidity from MODIS. *IEEE Trans. Geosci. Remote Sens.*, **41**, 442-458.
- Mace, G. G., Y. Zhang, S. Platnick, M. D. King, P. Minnis, and P. Yang, 2005: Evaluation of cirrus cloud properties from MODIS radiances using cloud properties derived from ground-based data collected at the ARM SGP site. *J. Appl. Meteorol.*, **44**, 221-240.
- Minnis, P., D. R. Doelling, L. Nguyen, and W. F. Miller, 2006: Assessment of the visible channel calibrations of the TRMM VIRS and MODIS on *Aqua* and *Terra*. Submitted to *J. Atmos. Oceanic Technol.*
- Minnis, P., D. P. Garber, D. F. Young, R. F. Arduini, and Y. Takano, 1998: Parameterization of reflectance and effective emittance for satellite remote sensing of cloud properties. *J. Atmos. Sci.*, **55**, 3313-3339.
- Minnis, P., P. W. Heck, D. F. Young, C. W. Fairall, and J. B. Snider, 1992: Stratocumulus cloud properties derived from simultaneous satellite and island-based instrumentation during FIRE. *J. Appl. Meteorol.*, **31**, 317-339.
- Minnis, P., et al., 1995: Cloud Optical Property Retrieval (Subsystem 4.3). "Clouds and the Earth's Radiant Energy System (CERES) Algorithm Theoretical Basis Document, Volume III: Cloud Analyses and Radiance Inversions (Subsystem 4)", *NASA RP 1376 Vol. 3*, pp. 135-176.
- Minnis, P., D. F. Young, S. Sun-Mack, P. W. Heck, D. R. Doelling, and Q. Z. Trepte, 2003: CERES cloud property retrievals from imagers on TRMM, Terra, and *Aqua*. *SPIE 10th Intl. Symp Remote Sens., Conf. Remote Sens. Clouds and Atmos.*, Barcelona, Spain, September 8-12, 37-48.
- Minnis, P., D. F. Young, B. A. Weilicki, S. Sun-Mack, Q. Z. Trepte, Y. Chen, P. W. Heck, and X. Dong, 2002: A global cloud database from VIRS and MODIS for CERES. *Proc. SPIE 3rd Intl. Asia-Pacific Environ. Remote Sensing Symp. 2002: Remote Sens. of Atmosphere, Ocean, Environment, and Space*, Hangzhou, China, October 23-27, Vol. 4891, 115-126.
- Minnis, P., D. F. Young, S. Sun-Mack, Q. Z. Trepte, R. R. Brown, S. Gibson, and P. Heck, 2004: Diurnal, seasonal, and interannual variations of cloud properties derived for CERES from imager data. *Proc. 13th AMS Conf. Satellite Oceanogr. and Meteorol.*, Norfolk, VA, Sept. 20-24, CD-ROM, P6.10.
- Platnick, S., J. Y. Li, M. D. King, H. Gerber, and P. V. Hobbs, A solar reflectance method for retrieving cloud optical thickness and droplet size over snow and ice surfaces. *J. Geophys. Res.*, **106**, 15185-15199, 2001.
- Sun-Mack, S., Y. Chen, T. D. Murray, P. Minnis, and D. F. Young, 1999: Visible clear-sky and near-infrared surface albedos derived from VIRS for CERES. *Proc. AMS 10th Conf. Atmos. Rad.*, Madison, WI, June 28 – July 2, 422-425.
- Sun-Mack, S., P. Minnis, Y. Chen, and R. F. Arduini, 2003: Clear-sky narrowband albedos derived from VIRS and MODIS. *SPIE 10th Intl. Symp Remote Sens., Conf. Remote Sens. Clouds and Atmos.*, Barcelona, Spain, September 8-12, 101-109.
- Sun-Mack, S., Y. Chen, Q. Z. Trepte, P. Minnis, E. Geier, and P. W. Heck, 2006: CERES cloud property database from VIRS and MODIS. *Proc. AMS 14th Conf. Satellite Meteorol. and Oceanog.*, Atlanta, GA, 29 Jan. - 2 Feb., CD-ROM, 5.3.
- Trepte, Q., Y. Chen, S. Sun-Mack, P. Minnis, D. F. Young, B. A. Baum, and P. W. Heck, 1999: Scene identification for the CERES cloud analysis subsystem. *Proc. AMS 10th Conf. Atmos. Rad.*, Madison, WI, June 28 – July 2, 169-172.
- Trepte, Q., P. Minnis, and R. F. Arduini, 2002: Daytime and nighttime polar cloud and snow identification using MODIS data. *Proc. SPIE 3rd Intl. Asia-Pacific*

Environ. Remote Sensing Symp. 2002: Remote Sens. of Atmosphere, Ocean, Environment, and Space, Hangzhou, China, October 23-27, Vol. 4891, 449-459.

Trepte, Q., P. Minnis, R. Palikonda, D. A. Spangenberg, and M. Haeffelin, 2006: Improved thin cirrus and terminator cloud detection in the CERES cloud mask.

Proc. AMS 12th Conf. Cloud Physics, Madison, WI, July 10-14, CD-ROM, P4.26.

Wielicki, B. A., et al., 1998: Clouds and the Earth's Radiant Energy System (CERES): Algorithm overview. *IEEE Trans. Geosci. Remote Sens.*, **36**, 1127-1141.